

REVIEW

Open Access



Perovskite oxides as transparent semiconductors: a review

Haiying He¹, Zhihao Yang^{1*}, Yonghang Xu¹, Andrew T. Smith^{2,3}, Guangguang Yang⁴ and Luyi Sun^{2,3*}

Abstract

Traditional transparent conducting oxides (TCOs) have been widely used for various optoelectronic applications, but have the trade-off between conductivity and transmittance. Recently, perovskite oxides, with structural and chemical stability, have exhibited excellent physical properties as new TCOs. We focus on SrVO₃-based perovskites with a high carrier concentration and BaSnO₃-based perovskites with a high mobility for n-type TCOs. In addition, p-type perovskites are discussed, which can serve as potential future options to couple with n-type perovskites to design full perovskite based devices.

Keywords: Perovskite oxide, Transparent conducting oxide, SrVO₃, BaSnO₃, Semiconductor

1 Introduction

Transparent conducting oxides (TCOs) are a group of unique materials for optoelectronic applications, including displays, solar cells, and light-emitting diodes [1–4]. High transmittance ($\geq 80\%$) in the visible spectrum, high conductivity, and high carrier mobility are required for transparent electronics. Various metal oxide materials, such as Sn-doped In₂O₃ (ITO) [5–7], F-doped SnO₂ (FTO) [8, 9], Sb-doped SnO₂ (ATO) [10, 11], and Al-doped ZnO (AZO) [12–15], have been investigated. Researchers have been developing these oxides to exhibit high performance by focusing on transmittance in the visible range, electrical conductivity at room temperature, stability in the working environment, high carrier mobility, and controlling conductive type.

Electrical conductivity is determined by $\sigma = en\mu = e^2\tau(\mathbf{n}/\mathbf{m}^*)$, where τ , \mathbf{n} , and \mathbf{m}^* are scattering time, carrier concentration, and electron effective mass, respectively. It is clear that the value of \mathbf{n}/\mathbf{m}^* is the key to achieve high performance of TCOs provided that the scattering time

is maximized [16]. Typical post-transition metal cations such as In³⁺ [7, 17], Zn²⁺ [18], and Sn⁴⁺ [19] have largely spread vacant s-orbitals to form the conduction band minimum (CBM) of TCOs, along with small effective masses. Among these materials, ITO has been widely used in industry thanks to its highest conductivity ($\sim 10^4 \text{ S}\cdot\text{cm}^{-1}$), along with an electron carrier concentration of the order of 10^{21} cm^{-3} [5, 20]. However, the carrier concentration is limited and the total scattering time of the carriers could be reduced due to the solubility limitation of the dopants as well as self-compensation [21–23]. Additionally, it is well-known that the markets for transparent devices are large but the critical raw material, Indium (In), is scarce on earth, which has led to high costs [24]. Substitution with ZnO- and SnO₂-based binary compounds has found success with optimized electrical performance, but this strongly depends on approaches of deposition and growing conditions [25]. It should be noted that it is difficult to deposit high performance impurity-doped metal oxide thin films. The key factors are to improve crystallinity by deposition methods and control an oxidizing atmosphere [25–27]. It was reported that AZO thin films deposited by pulsed laser deposition (PLD) showed an encouraging conductivity of the order of $10^4 \text{ S}\cdot\text{cm}^{-1}$ [15].

Carrier mobility (μ), defined as $\mu = e\tau/\mathbf{m}^*$, is another important factor for the high performance of transparent

*Correspondence: pvtech@qq.com; luyi.sun@uconn.edu

¹ School of Materials Science and Hydrogen Energy, Foshan University, Foshan 528000, China

² Polymer Program, Institute of Materials Science, University of Connecticut, Storrs, CT 06269, USA

Full list of author information is available at the end of the article

oxides. Conduction bands derived from widely spread metal *s* orbitals result in n-type conductivity and thus excellent electron carrier mobility, whose values range from 10 to 100 $\text{cm}^2 \cdot \text{V}^{-1} \cdot \text{s}^{-1}$. However, the applications of transparent oxides can hardly be further developed due to the lack of p-type counterparts for p-n heterojunctions [20, 28, 29] or other p-type devices like photovoltaics [3]. So far no efficient method has been created to introduce shallow acceptors and small hole effective mass due to strongly localized O 2p orbital derived from valence bands of metal oxides, though huge efforts have been made [30]. The carrier mobility of p-type TCOs cannot compare with those of n-type, even though high mobility values have been achieved from Cu-based materials [31, 32] at the sacrifice of hole carrier concentration.

ABO₃-based perovskite oxides are common in inorganic compounds. The ideal cubic perovskite structure (*Pm-3 m*) is composed of an A-site cation (an alkaline-earth, a rare-earth or an alkali element), B-site cation (a transition or post-transition metal element from periods 4, 5, or 6 in the periodic table), and oxygen anions. B-site cation sits at the center of BO₆ octahedron [65]. It should be noted that distortions are caused by cations of different radii, which results in octahedral tilting. The structure of perovskite oxides can remain stable even if A- or B-site cations are replaced by a large amount of other elements [33, 34]. Materials with a perovskite structure have drawn high attention for extensive research on a variety of physical properties, including superconductivity [35], metal-insulator transition [36], photovoltaic effect [37], transparent conductivity [38–43], magnetism [44], and ferroelectricity [37, 45]. In particular, using novel perovskite oxides to replace traditional binary TCO materials has become popular. Recently, Zhang et al. [16] reported that correlated metal compounds (e.g., SrVO₃ and CaVO₃), as transparent conductors, had an excellent carrier concentration ($> 2.2 \times 10^{22} \text{ cm}^{-3}$), an order of magnitude greater than that of ITO ($\sim 10^{21} \text{ cm}^{-3}$). Alkaline earth stannates (ASnO₃, A = Ca, Sr, Ba) have a wide bandgap ($\sim 3.0 \text{ eV}$), exhibiting highly transparent visible photovoltaic effective range and excellent electrical properties [46–50], i.e., a mobility up to 320 $\text{cm}^2 \cdot \text{V}^{-1} \cdot \text{s}^{-1}$ at room temperature [51, 52]. In contrary to stoichiometric perovskite oxides that are insulating, oxygen-deficient structures transform to semiconductor or conductor, i.e., oxygen vacancy also plays a role in electrical properties [53, 54]. Early research results have revealed high thermal stability of oxygen in perovskite materials [55, 56], thus avoiding the degradation in the oxide-based electronic devices.

On the other hand, it remains a challenge to achieve p-type conductivity by binary post-transition metal oxide because of strongly localized O 2p orbitals, resulting in

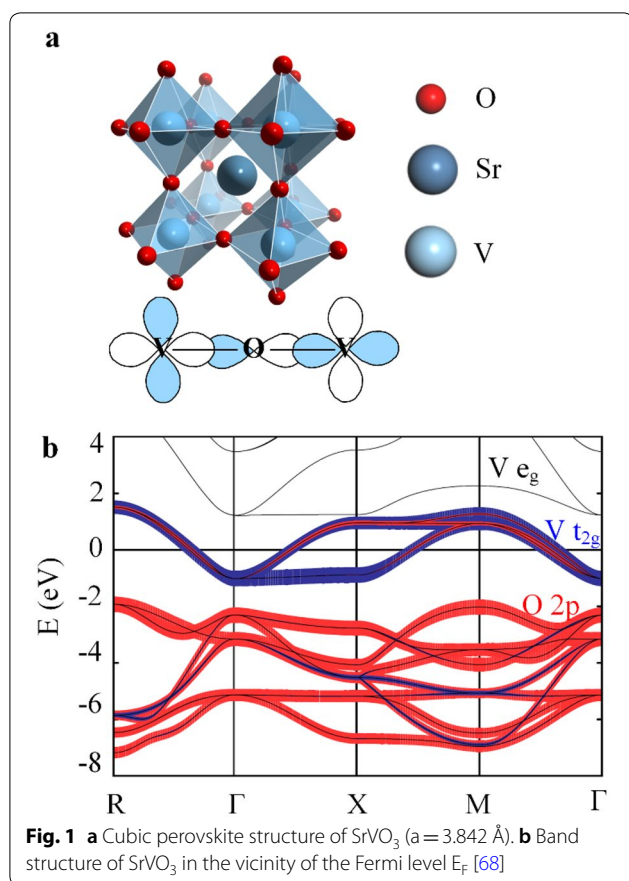
high formation energy of acceptor and large hole carrier masses. Fortunately, A or B sites can easily be replaced by other elements in perovskite oxides, thanks to the high chemical and structural stability. Stoichiometric strontium titanate (SrTiO₃, STO) is a group of highly transparent insulators ($E_g \sim 3.2 \text{ eV}$) that can be easily doped by Nb [57], La [58], or Sb [59] for n-type STO, or doped by Sc [60], and In [61] for p-type ones. Like “chemical modulation of the valence band” (CMVB), introduced by Hosono et al., partial replacement of Al for Sn in cubic perovskite-structures, SrSnO₃, can decrease the localization and generate holes in the valence [62]. Perovskite compounds such as La_{1-x}AlSnO₃ [62], La_{1-x}Sr_xCrO₃ [42, 63], La_{2/3}Sr_{1/3}VO₃ [33], SrTiO₃:Rh [64], etc., can be p-type TCO candidates, which demonstrate excellent electrical and optical properties. The new perovskite oxides not only balance the trade-off between conductivity and transmittance, but also show p-type characteristics. Development of p-type perovskite oxides are critical, along with n-type perovskites, to make full perovskite devices.

In this article, we review the novel TCO materials based on perovskite oxides. Section 2 discusses the crystal structure, electronic properties, fabrication methods of the SrVO₃- and BaSnO₃-based perovskites. SrVO₃ films inherit a high conductivity thanks to the high carrier concentration, even though they have a high effective mass. BaSnO₃-based perovskites have a high mobility. Section 3 describes the properties and impurity doping of p-type perovskite oxides. Due to their high chemical stability, perovskite oxides can be doped with A- or B-site.

2 n-Type perovskites

2.1 SrVO₃

Alkaline earth metal vanadium oxides with the AVO₃ (A = Ca, Sr, Ba) composition have a V⁴⁺ 3d¹ electronic configuration with a single electron in the partially filled t_{2g} band. The first-principle calculations showed three t_{2g} bands at the Fermi energy between -1.5 eV and 1.5 eV [66]. In this article, strontium vanadium oxide (SrVO₃, SVO), which has aroused widespread interest, is selected to illustrate that strongly correlated metal oxides are promising transparent conductive materials. SVO possesses cubic symmetry ($a = 3.842 \text{ \AA}$) with one V atom surrounded by six O atoms to form an octahedral configuration (Fig. 1a). The valence band maximum (VBM) is composed of O 2p orbitals, and the conduction band minimum (CBM) is composed of V 3d orbitals that can be split into e_g and t_{2g} states (Fig. 1b). The width of 3d bands is narrow enough ($W \approx 2\text{--}3 \text{ eV}$) so that the local Coulomb interaction between the electrons is particularly strong, causing electronic correlations [67].



SVO is an important strongly correlated metal oxide that has been extensively investigated in both theoretical [68–70] and experimental researches [71–73]. Recently, SVO has been reported as a transparent conductor because of its high electrical properties. Contrary to heavy doping to optimize physical properties in wide-bandgap semiconductors, Zhang et al. [16] demonstrated that novel materials with strong electron–electron

interactions had a higher carrier concentration in comparison with that of ITO. This kind of materials inherit a high conductivity ($\sim 10^4$ S·cm⁻¹) due to the higher carrier concentration ($\sim 10^{22}$ cm⁻³) although they have a high effective mass. In addition, SVO films show optical transmittance in the visible range due to lower plasma frequency ($\omega_p^* = 1.33$ eV), allowing them to be thinner, to increase optical transmittance in the visible spectrum range without suffering from surface scattering because of the much smaller electron mean free path ($EMFP = \hbar(3\pi^2)^{1/3}(\tau/n^{2/3})$ (n/m³)) in correlated metal oxides (SrVO₃, EMFP = 5.6 nm and CaVO₃, EMFP = 3.9 nm) [16] than other conductors, like Ag (EMFP = 52 nm) and Au (EMFP = 50 nm) [74, 75].

However, an inevitable problem is that the carrier mobility and transmittance of SVO is lower than ITO. The factors those affect the physical properties of the SVO thin films, including: (1) Film crystallinity. The SVO thin films with high performance are all crystal phase deposited on lattice-matching substrates, such as (LaAlO₃)_{0.3}(Sr₂AlTaO₆)_{0.7} (LSAT), SrTiO₃ (STO), NdGaO₃ (NGO), etc., as shown in Table 1, instead of on an amorphous substrate (glass or PET) or other substrates with a different crystal structure (Si, GaN, or Al₂O₃). Note that the properties of the films are not directly affected by the lattice mismatch, but mainly determined by lattice misfit between the SVO film ($a(\text{SVO})$) and the substrate (a_s), $f = [a_s - a(\text{SVO})] / a_s$. The f values between SVO bulk and LSAT (3.868 Å), STO (3.905 Å), and NGO (3.863 Å) substrates are +0.67%, +1.61%, and +0.54%, respectively. Under the same growth conditions, the carrier concentration (or mobility) of the SVO films on LSAT and NGO are close, with values of 2.14×10^{22} cm⁻³ (2.9 cm²·V⁻¹·s⁻¹) and 2.2×10^{22} cm⁻³ (3.3 cm²·V⁻¹·s⁻¹), respectively [76]. However, the resistivity of the SVO film grown on an LSAT substrate (70 μΩ·cm) is lower than that on

Table 1 Summary of the electrical properties of SrVO₃ thin films compared to ITO

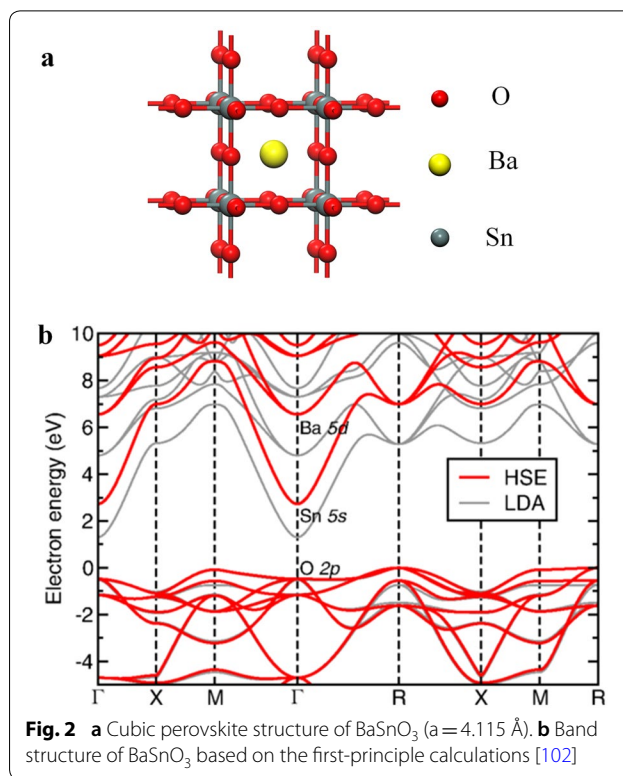
Substrate	Deposit methods	Mobility cm ² ·V ⁻¹ ·s ⁻¹	Carrier concentration cm ⁻³ (× 10 ²²)	Resistivity Ω·cm (× 10 ⁻⁵)	Ref.
Sn:In ₂ O ₃ (ITO) On glass substrate	Reactive e-beam evaporation	~30	0.08	~0.2	[6]
SrTiO ₃ (STO)	PLD	1.35	2.48	0.187	[78]
(LaAlO ₃) _{0.3} (Sr ₂ AlTaO ₆) _{0.7} (LSAT)	MBE	~10 ^a	2.26	2.8	[16]
(LaAlO ₃) _{0.3} (Sr ₂ AlTaO ₆) _{0.7} (LSAT)	Hybrid-MBE	~9 ^a	–	3	[43]
NdGaO ₃ (NGO)	PLD	8.3	2.4	3	[76]
(LaAlO ₃) _{0.3} (Sr ₂ AlTaO ₆) _{0.7} (LSAT)	PLD	~7 ^a	2.6	3.8	[76]
(LaAlO ₃) _{0.3} (Sr ₂ AlTaO ₆) _{0.7} (LSAT)	PLD	3.05	2.18	0.12~0.19	[80]
(LaAlO ₃) _{0.3} (Sr ₂ AlTaO ₆) _{0.7} (LSAT)	MBE	8.7	2.3	3.2	[81]
(LaAlO ₃) _{0.3} (Sr ₂ AlTaO ₆) _{0.7} (LSAT)	Sputtering	1.82	1.57	0.2	[84]

^a Values estimated graphically

a STO substrate ($90 \mu\Omega\cdot\text{cm}$) [77]. (2) Growing methods. To grow high quality thin films, various growing methods have been developed to deposit SVO films to achieve high performance, including pulsed laser deposition (PLD) [76–80], molecular beam epitaxy (MBE) [81], hybrid MBE [43, 82, 83], and radio frequency sputtering deposition (RF sputtering) [84]. These results show that preparation method has a great influence on the properties of the prepared films. This might be caused by the defects generated in the preparation process. For example, good stoichiometric SrVO_3 can be controlled by hybrid MBE, which can reduce the number of defects of perovskite-based oxide films [82, 83]. The resistivity ($28 \mu\Omega\cdot\text{cm}$) [16] of the SVO films grown by MBE measured at room temperature is lower than those grown by other deposition approaches like PLD (38 [79] and $120 \mu\Omega\cdot\text{cm}$ [80]).

An open question still facing SVO materials is if it will be one of the candidates to replace ITO in many optoelectronic devices. Except for high optical transmittance and high electrical properties, large area deposition, uniformity, and integration of oxide materials are essential. Amorphous materials have obvious advantages in the deposition of large area homogeneous films thanks to their anisotropy properties. Boileau et al. [80] investigated the optical and electrical properties of SVO films without long-range crystalline order. The resistivity and transmittance were found to depend on crystalline state. In the crystalline state, the transmittance reached ca. 80% for a 520 nm film and the resistivity was measured to be $1.2\sim 1.9 \times 10^{-4} \Omega\cdot\text{cm}$, while the electrical properties decreased sharply with a decreasing crystallinity and the resistivity increased by orders of magnitude. The crystallinity of SVO significantly affects the properties of the films, limiting their potential as an alternative to ITO. Besides, the mobility of carriers is low due to the high effective mass induced by strong electron–electron interaction.

Furthermore, the performance of SVO thin films is sensitive to oxygen pressure [77, 79, 85]. In general, SVO is grown under low oxygen pressure, which is different from other strongly correlated perovskite materials, such as LaNiO_3 and SrRuO_3 grown under high oxygen pressure conditions [86–88]. At a high oxygen pressure, V^{4+} can be easily oxidized into V^{5+} , indicating that optimization of oxygen pressure has a positive effect on film properties. It should be noted that the properties of the films prepared in vacuum are not optimal [77, 79]. Wang et al. achieved the highest conductivity at room temperature with an oxygen pressure of 1×10^{-5} mbar [77]. The effect of oxygen pressure on



the physical properties of thin films is still not completely clear and requires further investigation.

2.2 BaSnO_3

2.2.1 Theoretical calculation

The limitation of SVO films for wide applications is their low carrier mobility, which is just on the order of $10 \text{ cm}^2\cdot\text{V}^{-1}\cdot\text{s}^{-1}$. It is difficult to enhance the mobility because of high effective mass and anisotropic electron carrier transport path. In contrast to strongly correlated SVO, alkaline earth stannates (ASnO_3 , $A = \text{Ba}$, Sr , and Ca) have been reported to have a high mobility, particularly barium stannate (BaSnO_3). Unlike $\text{V} 3d$, $\text{Sn} 5s$ orbitals are isotropic and can still overlap to a large extent even in the amorphous state, without affecting the conductivity. Metal ions with $(n-1) d^{10}ns^0$ electronic configuration play a dominant role in high conductivity and high mobility of amorphous semiconductor materials [89, 90]. According to the literature, BaSnO_3 (belonging to the perovskite family), shows a wide band gap ($E_g > 3.1 \text{ eV}$) [91], a high thermal stability [55], and a high carrier mobility up to $320 \text{ cm}^2\cdot\text{V}^{-1}\cdot\text{s}^{-1}$ in single crystals at room temperature [51] and $70 \text{ cm}^2\cdot\text{V}^{-1}\cdot\text{s}^{-1}$ in epitaxial films [52], respectively. Caused by the high mobility, BaSnO_3 -based materials have been used as a semiconductor layer in oxide thin film transistors (TFTs) [92–95] and other

photoelectronic devices [96–98]. It should be mentioned that the mobility of BaSnO_3 is much higher than that of SrVO_3 . In contrast to CBM derived mainly from the localized V 3d states, the first-principle calculations showed that CBM is dominated by dispersive Sn 5s states (Fig. 2), leading to a smaller carrier effective mass [48, 99]. This is similar to other cations with a $(n-1)d^{10}ns^0$ electron configuration, such as In^{3+} , Zn^{2+} , and Ga^{3+} . Most effective masses of BaSnO_3 from the first-principle calculations are between 0.2 and $0.5m_0$ [38, 48, 96, 100, 101]. They are apparently smaller than titanium- or vanadium-based perovskites, e.g., BaTiO_3 ($5.3m_0$) [103], and SrVO_3 ($3.0m_0$) [76], but close to traditional semiconductors, such as Si ($0.27m_0$) [104], In_2O_3 ($0.35m_0$) [25], and SnO_2 ($0.25m_0$) [105]. The smallest value below $0.03m_0$ was reported by Moreira et al. with first-principle local density approximation (LDA) and generalized gradient approximations (GGA) calculations [106]. The small effective mass has been found in tin-based perovskites [48], including SrSnO_3 ($0.23m_0$), ZnSnO_3 ($0.17m_0$), and CdSnO_3 ($0.23m_0$). This indicates that cation Sn on B-site is critical to high mobility.

2.2.2 Crystalline BaSnO_3

High mobility has not been measured for stoichiometric BaSnO_3 and it is known that it is not caused by intrinsic defects, but obtained from La-doped BaSnO_3 . Negative defect formation energy indicates a high concentration of substituting La for Ba (La_{Ba}) in BaSnO_3 [107], while the charge-state transition energy level, $E[\text{La}_{\text{Ba}} (+/0)]$, with respect to CBM is just 0.046 eV, indicating La_{Ba} to be a shallow donor, which contributes one electron easily by the ionization of La atoms [48]. To be a good candidate for TCOs, the solubility of dopants should be high and the donor level should be shallow. High carrier mobility of $\text{Ba}_{1-x}\text{La}_x\text{SnO}_3$ ($x=0$ to 0.04) crystals were reported by Luo et al., when $x=0.02$ the highest mobility was about $103 \text{ cm}^2\cdot\text{V}^{-1}\cdot\text{s}^{-1}$ corresponding to a carrier concentration of $\sim 8\text{--}10 \times 10^{19} \text{ cm}^{-3}$ [108]. Kim et al. [51] enhanced the carrier mobility of (Ba, La) SnO_3 single crystals to the highest value so far of $320 \text{ cm}^2\cdot\text{V}^{-1}\cdot\text{s}^{-1}$. In the crystal structure of BaSnO_3 , tin atom is at the center of the octahedra (SnO_6) and the bond angle of Sn–O–Sn is $\sim 180^\circ$. When Ba is partially replaced by La, the defects (La_{Ba}) are located away from SnO_6 octahedra, causing a low disorder effect. In addition, at a doping concentration of $8 \times 10^{19} \text{ cm}^{-3}$, the mobility showed the highest value [51]. For single crystals, the mobility decreases with an increasing carrier concentration due to scattering. Therefore, a suitable doping level can reduce the dopant scattering

in comparison with high carrier concentrations ($> 10^{20} \text{ cm}^{-3}$). Phonon scattering also has an effect on carrier mobility, but such effect is less significant than that of dopant scattering.

2.2.3 Epitaxy-grown BaSnO_3 films

Compared to single crystals, the mobility value of La-doped BaSnO_3 epitaxial films is much lower due to grain boundaries and dislocations caused by lattice mismatch between (Ba, La) SnO_3 and the substrate [109]. To enhance the film mobility, researchers managed to grow La-doped BaSnO_3 epitaxial films on other cubic perovskites, such as $\text{SrTiO}_3(001)$ [51, 52, 110], $\text{SmScO}_3(110)$ [111], $\text{PrScO}_3(110)$ [112], $\text{TbScO}_3(110)$ [113], and $\text{DyScO}_3(001)$ [114]. The electron mobility was enhanced from 5.8 to $183 \text{ cm}^2\cdot\text{V}^{-1}\cdot\text{s}^{-1}$ at room temperature, as shown in Fig. 3. Furthermore, BaSnO_3 epitaxial films were grown on BaSnO_3 single crystal substrate with a mobility of $102 \text{ cm}^2\cdot\text{V}^{-1}\cdot\text{s}^{-1}$ [115]. The mobility can be increased from $\sim 37 \text{ cm}^2\cdot\text{V}^{-1}\cdot\text{s}^{-1}$ (without buffer) to $\sim 56 \text{ cm}^2\cdot\text{V}^{-1}\cdot\text{s}^{-1}$ at room temperature when a bilayer of $\text{BaSnO}_3/(\text{Sr,Ba})\text{SnO}_3$ was inserted as a buffer layer to reduce dislocation scattering [116]. Wang et al. [117] reported that La-doped BaSnO_3 films using SrTiO_3 buffer on Si(001) substrate showed a mobility of $128 \text{ cm}^2\cdot\text{V}^{-1}\cdot\text{s}^{-1}$ at room temperature. This result is remarkable, but the fabrication cost has been significantly increased. To address this issue, Sanchela et al. [118] developed to grow La-doped BaSnO_3 films under a highly oxidative ozone (O_3) atmosphere, achieving a balance between mobility ($115 \text{ cm}^2\cdot\text{V}^{-1}\cdot\text{s}^{-1}$) and processing cost.

2.2.4 Oxygen vacancy

The intrinsic point defect, oxygen vacancy (V_{O}), plays a crucial role in various oxide semiconductors, including ZnO , SnO_2 , and In_2O_3 . The first-principle calculated results show that the formation energy of V_{O} has a negative value in perovskite stannates [107], indicating defects will form spontaneously along with grown films. BaSnO_3 films with a high oxygen vacancy concentration were fabricated at low oxygen pressures [54, 119] and reducing conditions (Ar containing 5% H_2 gas) [120]. Oxygen vacancies are donor defects which could contribute twice as many electron carriers per single-unit defect. Experimentally, high n-type carrier concentrations have been reported under O-poor growth conditions [54, 121, 122]. Son and coworker [123] reported that the mobility of La-doped BaSnO_3 film was $78 \text{ cm}^2\cdot\text{V}^{-1}\cdot\text{s}^{-1}$ at room temperature by high-temperature annealing under a N_2 environment to generate V_{O} . Later, the same group enhanced the mobility

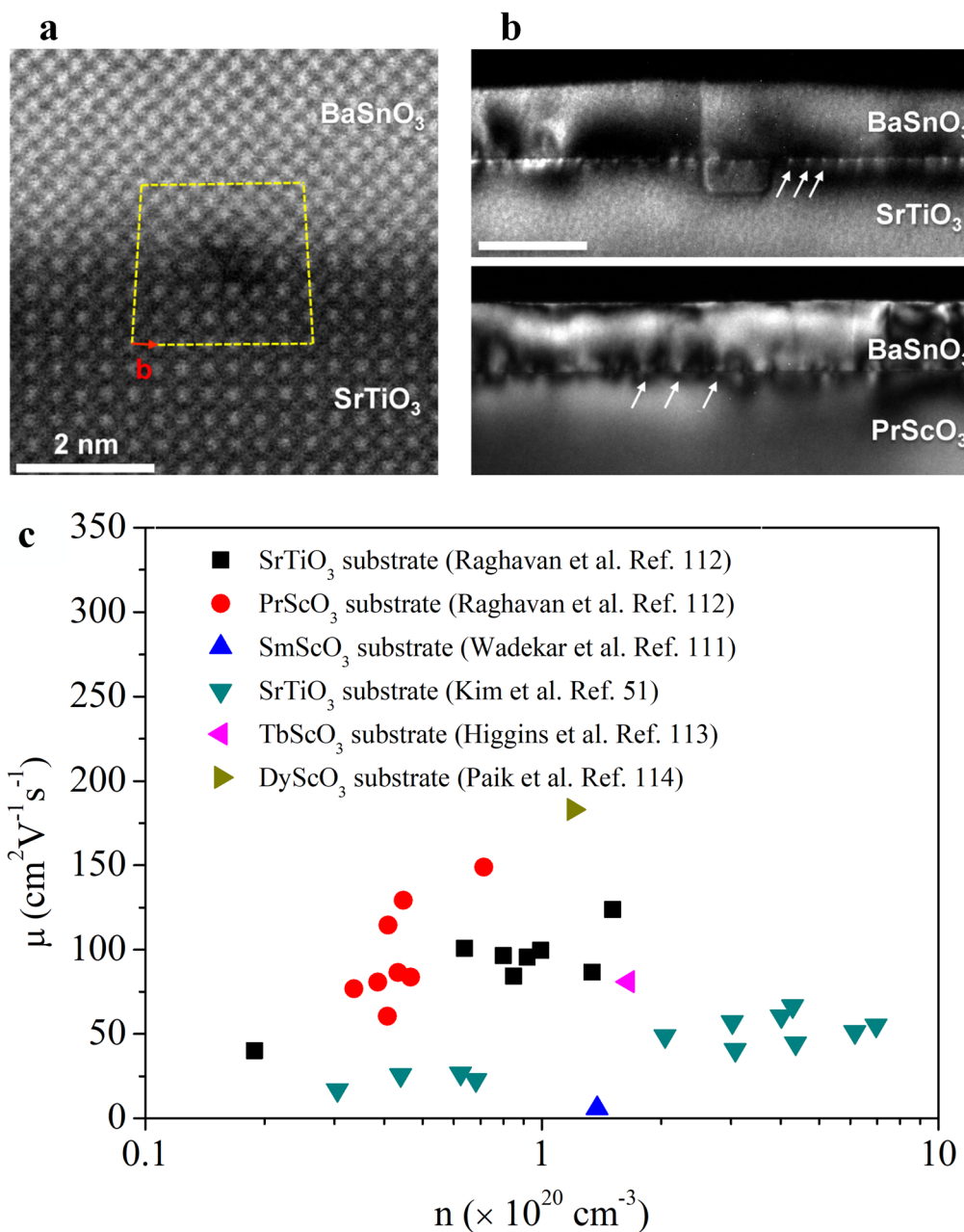


Fig. 3 **a** High-angle annular dark-field (HAADF)-STEM image of BaSnO₃/SrTiO₃ interface [112]. **b** Cross section dark-field TEM images of BaSnO₃ on SrTiO₃ (top) and PrScO₃ substrates (bottom) [112]. **c** Summary of the mobility of BaSnO₃ epitaxial films grown on SrTiO₃ [51, 112], SmScO₃ [111], PrScO₃ [112], TbScO₃ [113], and DyScO₃ [114] substrates

up to $122 \text{ cm}^2 \cdot \text{V}^{-1} \cdot \text{s}^{-1}$ by controlling the oxygen pressure using H₂ environment annealing [120]. In addition, it is known that oxygen vacancies could be generated by a vacuum annealing process in undoped BaSnO₃ films [124, 125]. Vacuum annealing methods have been reported to treat La-doped BaSnO₃ films on MgO

substrates with a carrier mobility of $101.6 \text{ cm}^2 \cdot \text{V}^{-1} \cdot \text{s}^{-1}$. The value was larger than that of the film deposited without annealing ($\sim 74 \text{ cm}^2 \cdot \text{V}^{-1} \cdot \text{s}^{-1}$) [126]. Therefore, it is important to investigate the effect of oxygen vacancies on physical properties of BaSnO₃ films.

3 p-Type perovskites

Conventional TCOs, including ZnO, SnO₂, and In₂O₃, typically exhibit n-type electronic conductivity, and are widely used in various fields. However, the lack of high performance p-type TCOs has limited their applications [127, 128]. In general, p-type TCOs were synthesized by acceptor doping to create holes in the valence band, but the hole concentration is usually not high enough due to recombination and strong localization [129, 130]. The conductivity and hole concentration suffer from doping bottlenecks, intrinsic defects, and the solubility limit of the acceptors. Although previous studies explored some approaches to change n-type TCOs to p-type ones, the hole carrier mobility is usually an order of magnitude lower than that of electron carrier. Moreover, Cu⁺-based oxides (CnMO₂, M=B, Al, Ga, In, Sc) with d¹⁰ configuration were used for intrinsically p-type doped materials [131]. Layered oxychalcogenides [132] and d⁶ spinel oxides [133] were reported to achieve p-type conductivity.

Due to their high chemical stability, ABO₃-based perovskite transition metal oxides are of great interest in p-type materials. Even with A- or B-site doping, it is still stable for perovskite structures. Lanthanide-based perovskite LaRhO₃ (LRO) with A-site doping (substituting La for Sr or Ca) was reported as a candidate for p-type semiconductors [134]. Nakamura et al. [135] reported a p-type single-crystalline LRO semiconductor and investigated the physical properties of a heterojunction, which was comprised of n-type Nb:SrTiO₃. The bandgap of p-type LRO was just 1.3 eV, as shown Fig. 4.

In comparison with Cu⁺-based p-type oxides, the localization of O 2p orbitals is reduced from hybridization with metal d orbitals using a method called “chemical modulation of the valence band” (CMVB) [136]. The correlated metal oxides, Cr₂O₃, V₂O₃, LaCrO₃, LaVO₃, and LaCoO₃, were identified to be p-type TCOs [33, 42, 137–139]. The VB consists of a hybridization between

O 2p orbitals and transition metal 3d orbitals, leading to a reduction of the hole localization at the top of VB. In A-site doped perovskites LaBO₃ (B=V, Cr, Co), the holes at the top of valence band (VB) could be introduced by replacing Sr²⁺ for La³⁺. Zhang et al. [42] grew a new p-type Sr-doped LaCrO₃ on SrTiO₃ substrate by molecular beam epitaxy. The conductivity was up to ~50 S cm⁻¹ due to a high hole carrier concentration of 7.5 × 10²¹ cm⁻³. In the periodic table, V element is located to the left side of Cr. Therefore, the size of the 3d wavefunction of V³⁺ is expanded, resulting in a smaller U (d–d Coulomb repulsion energy) in LaVO₃ than that of LaCrO₃ [140]. The conductivity of p-type La_{2/3}Sr_{1/3}VO₃ (LSVO) films was enhanced to nearly ~900 S·cm⁻¹ at room temperature [33]. Meanwhile, the films exhibited a high transmittance up to 70%, indicating that they possess the potential to be a high performance p-type TCO. Takashima et al. [139] grew p-type La_{0.67}Sr_{0.33}CoO₃ films on a SrTiO₃ substrate by controlling the oxygen atmosphere and prepared p-n heterostructure. Furthermore, p-BaSnO₃:K/n-BaSnO₃:La whole perovskite p-n junctions were reported, and results show that they are stable at elevated temperatures (up to 300 °C) [141].

With regard to B-site doped materials, researchers substitute tetravalent ions on B-site by trivalent ions to prepare p-type perovskite oxides. SrTi_{1-x}Sc_xO₃ is a p-type semiconductor with Sc³⁺ replacing Ti⁴⁺ in SrTiO₃. However, the acceptor levels were so deep that the holes were localized [60]. Guo et al. [142] reported In-doped SrTiO₃ films to create hole carriers and investigated the optical properties. The average transmittance is up to 80% in the visible region. For Al-doped SrSnO₃ (E_g > 3.9 eV), the transmittance was increased, too [62].

Perovskites BaSnO₃ and BaZrO₃ doped by trivalent elements (Ga, Sc, In, Y) are able to incorporate oxygen at low temperatures. The hole concentration decreases at elevated temperatures [143]. Wang et al. reported that Y-doped BaSnO₃ showed p-type behavior under a

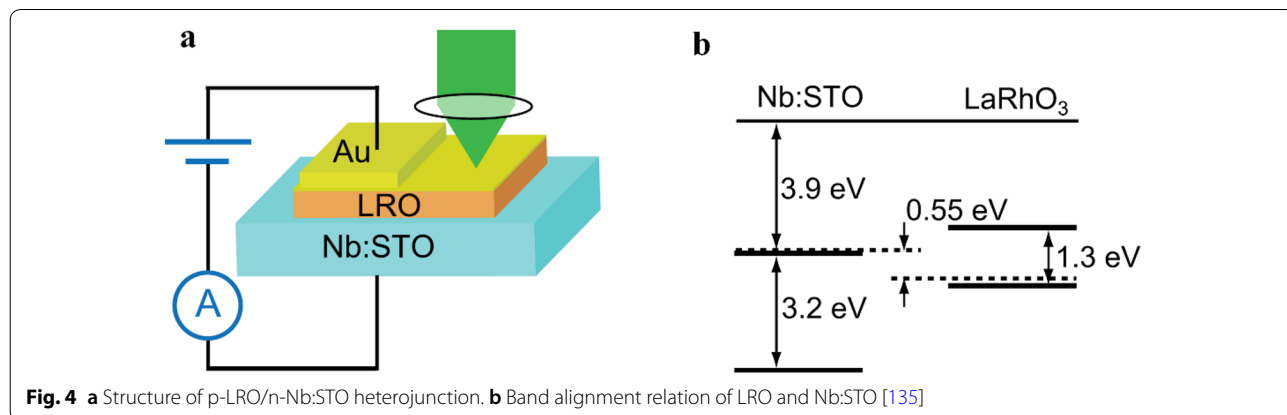


Fig. 4 a Structure of p-LRO/n-Nb:STO heterojunction. b Band alignment relation of LRO and Nb:STO [135]

controlled atmosphere [144]. It is well known that the electronic conductivity and Seebeck Coefficient of semi-conducting materials are measured by high-temperature sintering techniques. These procedures may lead to unreliable results such as changing transport properties from p- to n-type [145]. The holes induced by acceptor-doped perovskite oxides are compensated by intrinsic defects (oxygen vacancies) [146–148]. Acceptor-doped perovskite, BaSnO_3 , has also gained attention in various electrochemical devices [149, 150].

4 Conclusion and outlook

In this article, we comprehensively review the recent developments of perovskites with both high carrier concentration and mobility. SrVO_3 with strong electron–electron interactions exhibits a higher carrier concentration of $2.2 \times 10^{22} \text{ cm}^{-3}$ than that of ITO. It also maintains a high conductivity of $10^4 \text{ S}\cdot\text{cm}^{-1}$ and optical transmittance in the visible range by taking advantage of its lower plasma frequency ($\omega_p^* = 1.33 \text{ eV}$). The performance of SrVO_3 films are affected by crystallinity, mismatched substrate, and growth condition. A low resistivity of $28 \mu\Omega\cdot\text{cm}$ was achieved at room temperature in SVO films, which were grown by hybrid MBE in order to reduce the number of defects. Various lattice matched materials, including $(\text{LaAlO}_3)_{0.3}(\text{Sr}_2\text{AlTaO}_6)_{0.7}$ (LSAT), SrTiO_3 (STO), and NdGaO_3 (NGO) have been used as substrates to prepare SVO films. Meanwhile, the performances of SVO thin films are found sensitive to oxygen pressure. Due to the high effective mass, the carrier mobility is just on the order of $10 \text{ cm}^2\cdot\text{V}^{-1}\cdot\text{s}^{-1}$. On the other hand, BaSnO_3 -based perovskites with dispersive Sn 5 s states on the CBM, leading to a small carrier effective mass, have the highest carrier mobility of $320 \text{ cm}^2\cdot\text{V}^{-1}\cdot\text{s}^{-1}$ in the single crystals and $183 \text{ cm}^2\cdot\text{V}^{-1}\cdot\text{s}^{-1}$ in the epitaxial films at room temperature. It is easy to substitute Ba^{2+} by La^{3+} in BaSnO_3 to introduce electron carriers due to the low formation energy of La_{Ba} . Researchers have also managed to grow LBSO films on lattice matched substrates or insert a buffer layer between the LBSO and the substrate to enhance the carrier mobility. The performance of LBSO film is also affected by oxygen vacancy which could be controlled by depositional condition. Because of the high performance of SVO and LBSO films, they are expected to be excellent candidates of TCOs to further optimize the physical properties.

Moreover, perovskites with chemical and structural stability could be doped on A- or B-site by low valence metal ions to create stable holes in the valence band. Although various acceptor-doped perovskite oxides have been reported, their physical properties are still inferior to the corresponding n-type materials. It is necessary to

further optimize the performance of p-type perovskites. Furthermore, perovskite oxides can be doped as both n- and p-type conductors, so full perovskite devices might be possible eventually.

Acknowledgements

No.

Authors' contributions

HH, ZY, and LS planned for this review article. All the authors contributed to the drafting of sections. HH, ZY, AS and LS revised the manuscript. All authors read and approved the final manuscript.

Funding

Haiying He thanks the support by the National Natural Science Foundation of China (No. 11747090) and the Key Project of Department of Education of Guangdong Province (No. 2016GCZX008). Zhihao Yang thanks the support by the Guangdong Basic and Applied Basic Research Foundation (No. 2019B1515120008).

Availability of data and materials

No.

Competing interests

The authors declare that they have no competing interests.

Author details

¹ School of Materials Science and Hydrogen Energy, Foshan University, Foshan 528000, China. ² Polymer Program, Institute of Materials Science, University of Connecticut, Storrs, CT 06269, USA. ³ Department of Chemical & Biomolecular Engineering, University of Connecticut, Storrs, CT 06269, USA. ⁴ School of Electronic Information Engineering, Foshan University, Foshan 528000, China.

Received: 8 June 2020 Accepted: 15 September 2020

Published online: 02 October 2020

References

1. K. Nomura, H. Ohta, K. Ueda, T. Kamiya, M. Hirano, H. Hosono, *Science* **300**, 1269 (2003)
2. C.G. Granqvist, *Sol. Energ. Mat. Sol. C.* **91**, 1529 (2007)
3. E. Fortunato, D. Ginley, H. Hosono, D.C. Paine, *MRS Bull.* **32**, 242 (2007)
4. D.S. Ginley, C. Bright, *MRS Bull.* **25**, 15 (2000)
5. C.G. Granqvist, A. Hultåker, *Thin Solid Films* **411**, 1 (2002)
6. I. Hamberg, C.G. Granqvist, *J. Appl. Phys.* **60**, R123 (1986)
7. O. Mryasov, A.J. Freeman, *Phys. Rev. B* **64**, 233111 (2001)
8. V. Consonni, G. Rey, H. Roussel, B. Doisneau, E. Blanquet, D. Bellet, *Acta Mater.* **61**, 22 (2013)
9. G. Rey, C. Ternon, M. Modreanu, X. Mescot, V. Consonni, D. Bellet, *J. Appl. Phys.* **114**, 183713 (2013)
10. S.-Y. Lee, B.-O. Park, *Thin Solid Films* **510**, 154 (2006)
11. J. Montero, J. Herrero, C. Guillén, *Sol. Energ. Mat. Sol. C.* **94**, 612 (2010)
12. M. Chen, Z. Pei, C. Sun, J. Gong, R. Huang, L. Wen, *Mat. Sci. Eng. B* **85**, 212 (2001)
13. C. Guillen, J. Herrero, *Vacuum* **84**, 924 (2010)
14. M. Chen, X. Wang, Y. Yu, Z. Pei, X. Bai, C. Sun, R. Huang, L. Wen, *Appl. Surf. Sci.* **158**, 134 (2000)
15. H. Agura, A. Suzuki, T. Matsushita, T. Aoki, M. Okuda, *Thin Solid Films* **445**, 263 (2003)
16. L. Zhang, Y. Zhou, L. Guo, W. Zhao, A. Barnes, H.-T. Zhang, C. Eaton, Y. Zheng, M. Brahlek, H.F. Haneef, *Nat. Mater.* **15**, 204 (2016)
17. P. Erhart, A. Klein, R.G. Egdell, K. Albe, *Phys. Rev. B* **75**, 153205 (2007)
18. L. Li, W. Wang, H. Liu, X. Liu, Q. Song, S. Ren, *J. Phys. Chem. C* **113**, 8460 (2009)
19. Q.-J. Liu, Z.-T. Liu, L.-P. Feng, *Comp. Mater. Sci.* **47**, 1016 (2010)
20. K. Ellmer, *Nat. Photonics* **6**, 809 (2012)

21. A.J. Freeman, K.R. Poeppelmeier, T.O. Mason, R.P. Chang, T.J. Marks, *MRS Bull.* **25**, 45 (2000)
22. F. Tuomisto, V. Ranki, K. Saarinen, D.C. Look, *Phys. Rev. Lett.* **91**, 205502 (2003)
23. A. Janotti, C.G. Van de Walle, *Phys. Rev. B* **76**, 165202 (2007)
24. S. Glöser, L. Tercero Espinoza, C. Ganderberger, M. Faulstich, *Resources Policy* **44**, 35 (2015)
25. T. Minami, *Semicond. Sci. Technol.* **20**, S35 (2005)
26. U.S. Alaani, P. Shafer, A.T. N'Diaye, E. Arenholz, Y. Suzuki, *Appl. Phys. Lett.* **108**, 042106 (2016)
27. M.-L. Lin, J.-M. Huang, C.-S. Ku, C.-M. Lin, H.-Y. Lee, J.-Y. Juang, *J. Alloy. Compd.* **727**, 565 (2017)
28. H. Ohta, H. Hosono, *Mater. Today* **7**, 42 (2004)
29. H. Kawazoe, H. Yanagi, K. Ueda, H. Hosono, *MRS Bull.* **25**, 28 (2000)
30. K.H.L. Zhang, K. Xi, M.G. Blamire, R.G. Egdell, *J. Phys.: Condens. Matter* **28**, 383002 (2016)
31. K. Matsuzaki, K. Nomura, H. Yanagi, T. Kamiya, M. Hirano, H. Hosono, *Appl. Phys. Lett.* **93**, 202107 (2008)
32. M. Snure, A. Tiwari, *Appl. Phys. Lett.* **91**, 092123 (2007)
33. L. Hu, R. Wei, J. Yan, D. Wang, X. Tang, X. Luo, W. Song, J. Dai, X. Zhu, C. Zhang, *Adv. Electron. Mater.* **4**, 1700476 (2018)
34. B. Wang, W. Zhang, K. Yang, T. Liao, F. Li, Y. Cui, Y. Gao, B. Liu, *Ceram. Int.* **44**, 16051 (2018)
35. J. Biscaras, N. Bergeal, A. Kushwaha, T. Wolf, A. Rastogi, R.C. Budhani, J. Lesueur, *Nat. Commun.* **1**, 1 (2010)
36. A. Mercy, J. Bieder, J. Iñiguez, P. Ghosez, *Nat. Commun.* **8**, 1 (2017)
37. I. Grinberg, D.V. West, M. Torres, G. Gou, D.M. Stein, L. Wu, G. Chen, E.M. Gallo, A.R. Akbashev, P.K. Davies, J.E. Spanier, A.M. Rappe, *Nature* **503**, 509 (2013)
38. D.O. Scanlon, *Phys. Rev. B* **87**, 161201 (2013)
39. A. Prakash, P. Xu, A. Faghaninia, S. Shukla, J.W. Ager 3rd, C.S. Lo, B. Jalan, *Nat. Commun.* **8**, 15167 (2017)
40. J. Ravichandran, W. Siemons, H. Heijmerikx, M. Huijben, A. Majumdar, R. Ramesh, *Chem. Mater.* **22**, 3983 (2010)
41. Y. Du, C. Li, K.H.L. Zhang, M.E. McBriarty, S.R. Spurgeon, H.S. Mehta, D. Wu, S.A. Chambers, *Appl. Phys. Lett.* **111**, 063501 (2017)
42. K.H. Zhang, Y. Du, A. Papadogianni, O. Bierwagen, S. Sallis, L.F. Piper, M.E. Bowden, V. Shutthanandan, P.V. Sushko, S.A. Chambers, *Adv. Mater.* **27**, 5191 (2015)
43. J.A. Moyer, C. Eaton, R. Engel-Herbert, *Adv. Mater.* **25**, 3578 (2013)
44. M. Grisolia, J. Varignon, G. Sanchez-Santolino, A. Arora, S. Valencia, M. Varela, R. Abrudan, E. Weschke, E. Schierle, J. Rault, *Nat. Phys.* **12**, 484 (2016)
45. J. Haeni, P. Irvin, W. Chang, R. Uecker, P. Reiche, Y. Li, S. Choudhury, W. Tian, M. Hawley, B. Craigo, *Nature* **430**, 758 (2004)
46. M.A. Riza, M.A. Ibrahim, U.C. Ahamefula, M.A. Mat Teridi, N. Ahmad Ludin, S. Sepeai, K. Sopian, *Sol. Energy* **137**, 371 (2016)
47. E. Moreira, J.M. Henriques, D.L. Azevedo, E.W.S. Caetano, V.N. Freire, E.L. Albuquerque, *J. Solid State Chem.* **184**, 921 (2011)
48. H.-R. Liu, J.-H. Yang, H.J. Xiang, X.G. Gong, S.-H. Wei, *Appl. Phys. Lett.* **102**, 112109 (2013)
49. Q. Liu, J. Liu, B. Li, H. Li, G. Zhu, K. Dai, Z. Liu, P. Zhang, J. Dai, *Appl. Phys. Lett.* **101**, 241901 (2012)
50. E. Baba, D. Kan, Y. Yamada, M. Haruta, H. Kurata, Y. Kanemitsu, Y. Shimakawa, *J. Phys. D Appl. Phys.* **48**, 455106 (2015)
51. H.J. Kim, U. Kim, H.M. Kim, T.H. Kim, H.S. Mun, B.-G. Jeon, K.T. Hong, W.-J. Lee, C. Ju, K.H. Kim, *Appl. Phys. Express* **5**, 061102 (2012)
52. H.J. Kim, U. Kim, T.H. Kim, J. Kim, H.M. Kim, B.-G. Jeon, W.-J. Lee, H.S. Mun, K.T. Hong, J. Yu, *Phys. Rev. B* **86**, 165205 (2012)
53. R. Perez-Casero, J. Perriere, A. Gutierrez-Llorente, D. Defourneau, E. Milion, W. Seiler, L. Soriano, *Phys. Rev. B* **75**, 165317 (2007)
54. H.M.I. Jaim, S. Lee, X. Zhang, I. Takeuchi, *Appl. Phys. Lett.* **111**, 172102 (2017)
55. W.J. Lee, H.J. Kim, J. Kang, D.H. Jang, T.H. Kim, J.H. Lee, K.H. Kim, *Annu. Rev. Mater. Res.* **47**, 391 (2017)
56. W.J. Lee, H.J. Kim, E. Sohn, H.M. Kim, T.H. Kim, K. Char, J.H. Kim, K.H. Kim, *Phys. Status Solidi A* **212**, 1487 (2015)
57. K.G. Rana, V. Khikhlovskiy, T. Banerjee, *Appl. Phys. Lett.* **100**, 213502 (2012)
58. M. Choi, A.B. Posadas, C.A. Rodriguez, A. O'Hara, H. Seinige, A.J. Kellock, M.M. Frank, M. Tsoi, S. Zollner, V. Narayanan, *J. Appl. Phys.* **116**, 043705 (2014)
59. H.H. Wang, F. Chen, S.Y. Dai, T. Zhao, H.B. Lu, D.F. Cui, Y.L. Zhou, Z.H. Chen, G.Z. Yang, *Appl. Phys. Lett.* **78**, 1676 (2001)
60. T. Higuchi, T. Tsukamoto, S. Yamaguchi, K. Kobayashi, N. Sata, M. Ishigame, S. Shin, *Nucl. Instrum. Meth. B* **199**, 255 (2003)
61. J.N. Yun, Z.Y. Zhang, *Acta Phys. Chim. Sin.* **26**, 751 (2010)
62. L.B. Amor, B. Belgacem, J.S. Filhol, M.L. Doublet, M.B. Yahia, R.B. Hassen, *Chem Commun* **56**, 2566 (2020)
63. K.H.L. Zhang, Y. Du, P.V. Sushko, M.E. Bowden, V. Shutthanandan, S. Sallis, L.F.J. Piper, S.A. Chambers, *Phys. Rev. B* **91**, 155129 (2015)
64. K. Iwashina, A. Kudo, *J. Am. Chem. Soc.* **133**, 13272 (2011)
65. A. Kubacka, M. Fernández-García, G. Colón, *Chem. Rev.* **112**, 1555 (2012)
66. I.A. Nekrasov, K. Held, G. Keller, D.E. Kondakov, T. Pruschke, M. Kollar, O.K. Andersen, V.I. Anisimov, D. Vollhardt, *Phys. Rev. B* **73**, 155112 (2006)
67. I. Nekrasov, G. Keller, D. Kondakov, A. Kozhevnikov, T. Pruschke, K. Held, D. Vollhardt, V. Anisimov, *Phys. Rev. B* **72**, 155106 (2005)
68. M. Karolak, T. Wehling, F. Lechermann, A. Lichtenstein, *J. Phys. Condens. Matter* **23**, 085601 (2011)
69. M. Casula, A. Rubtsov, S. Biermann, *Phys. Rev. B* **85**, 035115 (2012)
70. H. Lee, K. Foyevtsova, J. Ferber, M. Aichhorn, H.O. Jeschke, R. Valenti, *Phys. Rev. B* **85**, 165103 (2012)
71. T. Yoshida, M. Hashimoto, T. Takizawa, A. Fujimori, M. Kubota, K. Ono, H. Eisaki, *Phys. Rev. B* **82**, 085119 (2010)
72. K. Yoshimatsu, K. Horiba, H. Kumigashira, T. Yoshida, A. Fujimori, M. Oshima, *Science* **333**, 319 (2011)
73. S. Aizaki, T. Yoshida, K. Yoshimatsu, M. Takizawa, M. Minohara, S. Ideta, A. Fujimori, K. Gupta, P. Mahadevan, K. Horiba, *Phys. Rev. Lett.* **109**, 056401 (2012)
74. B. O'Connor, C. Haughn, K.-H. An, K.P. Pipe, M. Shtein, *Appl. Phys. Lett.* **93**, 223304 (2008)
75. K.R. Poeppelmeier, J.M. Rondinelli, *Nat. Mater.* **15**, 132 (2016)
76. M. Mirjole, F. Sánchez, J. Fontcuberta, *Adv. Funct. Mater.* **29**, 1808432 (2019)
77. J. Wang, G. Rijnders, G. Koster, *Appl. Phys. Lett.* **113**, 223103 (2018)
78. A. Boileau, A. Cheikh, A. Fouchet, A. David, C. Labbé, P. Marie, F. Gourbilleau, U. Lüders, *Adv. Opt. Mater.* **7**, 1801516 (2019)
79. B. Bérimi, V. Demange, M. Bouttemy, E. Popova, N. Keller, Y. Dumont, A. Fouchet, *Adv. Mater. Interf.* **3**, 1600274 (2016)
80. A. Boileau, A. Cheikh, A. Fouchet, A. David, R. Escobar-Galindo, C. Labbe, P. Marie, F. Gourbilleau, U. Lüders, *Appl. Phys. Lett.* **112**, 021905 (2018)
81. L. Shoham, M. Baskin, M.G. Han, Y. Zhu, L. Kornblum, *Adv. Electron. Mater.* **6**, 1900584 (2020)
82. M. Brahlek, L. Zhang, C. Eaton, H.-T. Zhang, R. Engel-Herbert, *Appl. Phys. Lett.* **107**, 143108 (2015)
83. C. Eaton, J.A. Moyer, H.M. Alipour, E.D. Grimley, M. Brahlek, J.M. LeBeau, R. Engel-Herbert, *J. Vac. Sci. Technol. A* **33**, 061504 (2015)
84. D.H. Jung, H.S. So, H. Lee, J. Vac. Sci. Technol. **A 37**, 021507 (2019)
85. A. Kumar, S. Maurya, S. Chawla, S. Patwardhan, B. Kavaipatti, *Appl. Phys. Lett.* **114**, 212103 (2019)
86. H.N. Lee, H.M. Christen, M.F. Chisholm, C.M. Rouleau, D.H. Lowndes, *Appl. Phys. Lett.* **84**, 4107 (2004)
87. G. Rijnders, D.H. Blank, J. Choi, C.-B. Eom, *Appl. Phys. Lett.* **84**, 505 (2004)
88. B. Berini, W. Noun, Y. Dumont, E. Popova, N. Keller, *J. Appl. Phys.* **101**, 023529 (2007)
89. M. Orita, H. Ohta, M. Hirano, S. Narushima, H. Hosono, *Philosophical Magazine B* **81**, 501 (2001)
90. H. Yabuta, M. Sano, K. Abe, T. Aiba, T. Den, H. Kumomi, K. Nomura, T. Kamiya, H. Hosono, *Appl. Phys. Lett.* **89**, 112123 (2006)
91. H. Mizoguchi, H.W. Eng, P.M. Woodward, *Inorg. Chem.* **43**, 1667 (2004)
92. C. Park, U. Kim, C.J. Ju, J.S. Park, Y.M. Kim, K. Char, *Appl. Phys. Lett.* **105**, 203503 (2014)
93. J. Shin, Y.M. Kim, Y. Kim, C. Park, K. Char, *Appl. Phys. Lett.* **109**, 262102 (2016)
94. U. Kim, C. Park, T. Ha, Y.M. Kim, N. Kim, C. Ju, J. Park, J. Yu, J.H. Kim, K. Char, *Appl. Phys. Lett.* **3**, 036101 (2015)
95. Y.M. Kim, C. Park, U. Kim, C. Ju, K. Char, *Appl. Phys. Express* **9**, 011201 (2015)
96. K. Krishnaswamy, L. Bjaalie, B. Himmetoglu, A. Janotti, L. Gordon, C.G.V.d. Walle, *Appl. Phys. Lett.* **108**, 083501 (2016)

97. K. Fujiwara, K. Nishihara, J. Shiogai, A. Tsukazaki, *Appl. Phys. Lett.* **110**, 203503 (2017)
98. J. Yue, A. Prakash, M.C. Robbins, S.J. Koester, B. Jalan, A.C.S. *Appl. Mater. Inter.* **10**, 21061 (2018)
99. A.V. Sanchela, T. Onozato, B. Feng, Y. Ikuhara, H. Ohta, *Phys. Rev. Mater.* **1**, 034603 (2017)
100. B.G. Kim, J.Y. Jo, S.W. Cheong, *J. Solid State Chem.* **197**, 134 (2013)
101. S. Dabaghmanesh, R. Saniz, M.N. Amini, D. Lamoen, B. Partoens, *J. Phys.: Condens. Matter* **25**, 415503 (2013)
102. B. Monserrat, C.E. Dreyer, K.M. Rabe, *Phys. Rev. B* **97**, 104310 (2018)
103. W. Wunderlich, H. Ohta, K. Koumoto, *Physica B* **404**, 2202 (2009)
104. D.M. Riffe, *JOSA B* **19**, 1092 (2002)
105. F. Simonis, M. Van Der Leij, C. Hoogendoorn, *Sol. Ene. Mater.* **1**, 221 (1979)
106. E. Moreira, J.M. Henriques, D.L. Azevedo, E.W.S. Caetano, V.N. Freire, U.L. Fulco, E.L. Albuquerque, *J. Appl. Phys.* **112**, 043703 (2012)
107. L. Weston, L. Bjaalie, K. Krishnaswamy, C. Van de Walle, *Phys. Rev. B* **97**, 054112 (2018)
108. X. Luo, Y.S. Oh, A. Sirenko, P. Gao, T.A. Tyson, K. Char, S.W. Cheong, *Appl. Phys. Lett.* **100**, 172112 (2012)
109. H. Mun, U. Kim, H.M. Kim, C. Park, T.H. Kim, H.J. Kim, K.H. Kim, K. Char, *Appl. Phys. Lett.* **102**, 252105 (2013)
110. K. Miura, D. Kiriya, T. Yoshimura, A. Ashida, N. Fujimura, *Phys. Status Solidi A* **216**, 1700800 (2019)
111. P.V. Wadekar, J. Alaria, M. O'Sullivan, N.L.O. Flack, T.D. Manning, L.J. Phillips, K. Durose, O. Lozano, S. Lucas, J.B. Claridge, M.J. Rosseinsky, *Appl. Phys. Lett.* **105**, 052104 (2014)
112. S. Raghavan, T. Schumann, H. Kim, J.Y. Zhang, T.A. Cain, S. Stemmer, *APL Mater.* **4**, 016106 (2016)
113. Z. Lebens-Higgins, D.O. Scanlon, H. Paik, S. Sallis, Y. Nie, M. Uchida, N.F. Quackenbush, M.J. Wahila, G.E. Sterbinsky, D.A. Arena, J.C. Woicik, D.G. Schlom, L.F.J. Piper, *Phys. Rev. Lett.* **116**, 027602 (2016)
114. H. Paik, Z. Chen, E. Lochocki, A. Seidner, H. Verma, N. Tanen, J. Park, M. Uchida, S. Shang, B.-C. Zhou, *APL Mater.* **5**, 116107 (2017)
115. W.-J. Lee, H.J. Kim, E. Sohn, T.H. Kim, J.-Y. Park, W. Park, H. Jeong, T. Lee, J.H. Kim, K.-Y. Choi, K.H. Kim, *Appl. Phys. Lett.* **108**, 082105 (2016)
116. J. Shiogai, K. Nishihara, K. Sato, A. Tsukazaki, *AIP Adv.* **6**, 065305 (2016)
117. Z. Wang, H. Paik, Z. Chen, D.A. Muller, D.G. Schlom, *APL Mater.* **7**, 022520 (2019)
118. A.V. Sanchela, M. Wei, J. Lee, G. Kim, H. Jeon, B. Feng, Y. Ikuhara, H.J. Cho, H. Ohta, *J. Mater. Chem. C* **7**, 5797 (2019)
119. A. Tiwari, M.S. Wong, *Thin Solid Films* **703**, 137986 (2020)
120. D. Yoon, S. Yu, J. Son, *NPG Asia Mater.* **10**, 363 (2018)
121. Q. Liu, J. Dai, Y. Zhang, H. Li, B. Li, Z. Liu, W. Wang, *J. Alloy. Compd.* **655**, 389 (2016)
122. I.A. Alagdal, A.R. West, *J. Mater. Chem. C* **4**, 4770 (2016)
123. S. Yu, D. Yoon, J. Son, *Appl. Phys. Lett.* **108**, 262101 (2016)
124. K. Ganguly, A. Prakash, B. Jalan, C. Leighton, *APL Mater.* **5**, 056102 (2017)
125. K. Ganguly, P. Ambwani, P. Xu, J.S. Jeong, K.A. Mkhoyan, C. Leighton, B. Jalan, *APL Mater.* **3**, 062509 (2015)
126. H.J. Cho, T. Onozato, M. Wei, A. Sanchela, H. Ohta, *APL Mater.* **7**, 022507 (2019)
127. G. Hautier, A. Miglio, G. Ceder, G.-M. Rignanese, X. Gonze, *Nat. Commun.* **4**, 2292 (2013)
128. R. Woods-Robinson, D. Broberg, A. Faghaninia, A. Jain, S.S. Dwaraknath, K.A. Persson, *Chem. Mater.* **30**, 8375 (2018)
129. J.L. Lyons, A. Janotti, C.G.V.d. Walle, *Appl. Phys. Lett.* **95**, 252105 (2009)
130. J.C. Fan, K.M. Sreekanth, Z. Xie, S.L. Chang, K.V. Rao, *Prog. Mater. Sci.* **58**, 874 (2013)
131. B.S. Li, K. Akimoto, A. Shen, *J. Cryst. Growth* **311**, 1102 (2009)
132. K. Ueda, S. Inoue, S. Hirose, H. Kawazoe, H. Hosono, *Appl. Phys. Lett.* **77**, 2701 (2000)
133. S. Narushima, H. Mizoguchi, K.-I. Shimizu, K. Ueda, H. Ohta, M. Hirano, T. Kamiya, H. Hosono, *Adv. Mater.* **15**, 1409 (2003)
134. T. Nakamura, T. Shimura, M. Itoh, Y. Takeda, *J. Solid State Chem.* **103**, 523 (1993)
135. M. Nakamura, Y. Krockenberger, J. Fujioka, M. Kawasaki, Y. Tokura, *Appl. Phys. Lett.* **106**, 072103 (2015)
136. H. Kawazoe, M. Yasukawa, H. Hyodo, M. Kurita, H. Yanagi, H. Hosono, *Nature* **389**, 939 (1997)
137. E. Arca, K. Fleischer, I.V. Shvets, *Appl. Phys. Lett.* **99**, 111910 (2011)
138. L. Hu, M. Zhao, S. Liang, D. Song, R. Wei, X. Tang, W. Song, J. Dai, G. He, C. Zhang, *Phys. Rev. Appl.* **12**, 044035 (2019)
139. H. Takashima, N. Kikuchi, H. Kawanaka, K. Tonooka, Y. Aiura, *Appl. Surf. Sci.* **422**, 869 (2017)
140. M. Imada, A. Fujimori, Y. Tokura, *Rev. Mod. Phys.* **70**, 1039 (1998)
141. H.M. Kim, U. Kim, C. Park, H. Kwon, K. Char, *APL Mater.* **4**, 056105 (2016)
142. H. Guo, L. Liu, Y. Fei, W. Xiang, H. Lü, S. Dai, Y. Zhou, Z. Chen, *J. Appl. Phys.* **94**, 4558 (2003)
143. E. Bévilion, G. Dezanneau, G. Geneste, *Physical Review B* **83**, 174101 (2011)
144. Y. Wang, A. Chesnaud, E. Bevilion, G. Dezanneau, *Solid State Ionics* **214**, 45 (2012)
145. S. Singh, P. Singh, O. Parkash, D. Kumar, *Adv. Appl. Ceram.* **106**, 231 (2007)
146. A. Zunger, *Appl. Phys. Lett.* **83**, 57 (2003)
147. J. Robertson, S.J. Clark, *Physical Review B* **83**, 075205 (2011)
148. D.O. Scanlon, G.W. Watson, *J. Mater. Chem.* **22**, 25236 (2012)
149. S. Choi, C.J. Kucharczyk, Y. Liang, X. Zhang, I. Takeuchi, H.-I. Ji, S.M. Haile, *Nature Energy* **3**, 202 (2018)
150. L.P. Putilov, A.K. Demin, V.I. Tsidilkovski, P. Tsiakaras, *Appl. Energy* **242**, 1448 (2019)

Publisher's Note

Springer Nature remains neutral with regard to jurisdictional claims in published maps and institutional affiliations.

Submit your manuscript to a SpringerOpen® journal and benefit from:

- Convenient online submission
- Rigorous peer review
- Open access: articles freely available online
- High visibility within the field
- Retaining the copyright to your article

Submit your next manuscript at ► [springeropen.com](https://www.springeropen.com)